Science Press

ARTICLE

Multimodal Distribution of γ′ Phase and Effect on Hot Deformation in a Wrought Nickel Base Superalloy

Han Guoming[1],   Li Fei[1],   Sun Baode[1,2]

[1]Shanghai Key Laboratory of Advanced High-temperature Materials and Precision Forming, Shanghai Jiao Tong University, Shanghai 200240, China; [2]State Key Laboratory of Metal Matrix Composites, Shanghai Jiao Tong University, Shanghai 200240, China

Abstract: The microstructural evolution of different generations of γ′ precipitates during various heat treatment processes of a nickel base superalloy has been investigated. After solutionizing in the single γ phase field, continuous cooling, interrupted cooling and isothermal annealing tests were performed and the precipitates was characterized by scanning electron microscopy. Results show that a monomodal size distribution of the secondary γ′ precipitates can be achieved at a very high cooling rate in the continuous cooling process. With the decrease of the cooling rate, the secondary γ′ precipitates grow gradually and gather together to form a flowery morphology. When the secondary supersaturation is developed in the vicinity of the secondary γ′ precipitates during isothermal annealing, the water-quenched tertiary γ′ precipitates are produced and result in a bimodal size distribution of γ′ precipitates with the larger secondary precipitates. Furthermore, the effects of the secondary γ′ particle growth on the hot deformation were also discussed.

Key words: wrought superalloy; γ′ precipitate; heat treatment; hot deformation

The nickel-based superalloys are widely used in a variety of applications requiring strength at high temperatures. Most of these alloys highly derive superior mechanical properties largely from the formation of typical γ/γ′ microstructures, where the γ′ phase with an ordered $L1_2$ Ni_3Al type structure is dispersed within a nickel-rich disordered γ matrix[1-4]. This structure provides a large amount of strengthening via γ′ precipitation hardening and therefore the γ′ characteristics such as the volume fraction, size distribution and morphologies have a profound effect on the properties of the superalloys[5-10]. Usually, the γ′ precipitates are classified as primary, secondary and tertiary γ′ according to the corresponding distribution and size in the polycrystalline turbine disc superalloys[11]. The primary γ′ particles located on grain boundaries and undissolved during the solutioning stage prevent the growth of γ grains during heat treatments. The secondary γ′ precipitates or namely cooling γ′ precipitates, which are larger than the tertiary γ′ precipitates and become intragranular upon quenching, form a bimodal microstructure with the tertiary γ′ precipitates produced

by aging treatments. It has been found that the bimodal size distributions of the γ′ precipitates are responsible for the high strength of the superalloys, and particularly creep strength is sensitive to the size and volume fraction of the tertiary γ′ precipitates[11, 12-14]. Consequently, an investigation of the factors affecting the bimodal size distribution and evolution of the γ′ precipitates seems extremely important.

The bimodal microstructures are usually formed by complex multiple heat treatments. However, recent experiments have shown that bimodal size can be obtained by two successive nucleations under continuous cooling conditions[13, 15-17]. Several studies have been focused on the effects of different single cooling profiles to explain the varied microstructural development according to multiple nucleation events during the linear cooling or subsequent quenching at different interrupted temperatures[17-19]. It is considered that the precipitation of γ′ is preceded by the development of a supersaturated γ-phase solid solution and affected by cooling rates employed. For faster cooling rates, such as water quenching from the

high temperature single γ phase field, a monomodal size distribution of the fine γ' precipitates can be produced. These precipitates display spherical morphology and their density is quite high, which is controlled by the nucleation kinetics of the fully supersaturated γ phase. In contrast, relatively slower cooling rates lead to the formation of multi-modal distribution of the γ' particle sizes, in which each size fraction is precipitated at different temperatures and from a different chemistry γ phase. The initial burst of nucleation, occurring at lower undercoolings, leads to the first generation of γ' precipitates. Subsequent bursts of nucleation are controlled at higher undercoolings as a result of the initial precipitation, cooling paths, new γ' phase nucleation kinetics and diffusion growth kinetics of the previously precipitated γ'. Since the barrier to nucleation is low for the γ', the nucleation process is assumed to be fast. On the other hand, the microstructural development under non-isothermal conditions involves nucleation, growth, and coarsening, in which the three mechanisms are often overlapping and even competing[13, 20-22]. Therefore, in addition to nucleation of γ' phase, growth or coarsening of γ' precipitates were taken as the mechanism controlling the γ' size during heat treatment. Particularly, the γ' precipitates produced through the first burst of nucleation under slower cooling rates play a critical role for the bimodal or multimodal distributions of the γ' particles.

In the present study, the effects of cooling rate and annealing time at certain temperatures on the size distribution and morphological evolution of the γ' particles are examined. The main objective of this research is to explain the microstructural development of the γ' precipitates during continuous cooling, interrupted cooling and isothermal annealing. Furthermore, the effects of the secondary γ' precipitates on the hot deformation behavior are also discussed.

1　Experiment

The material used in this investigation has a composition of 49.7Ni-15.3Cr-22.0Co-6.0Ti-4.8Al-1.6Mo-0.5W, all in at%. Samples with a size of about 10 mm × 10 mm × 5 mm were cut from a forged billet. Before all experimental tests, in order to dissolve all γ' particles and form one single-phase solid solution, all samples were homogenized at 1220 °C for 8 h and then air-cooled down to the room temperature.

To explore the effects of cooling on the γ' size and distribution, samples for continuous cooling tests were cooled at three different rates of 1 °C/min, 300 °C/min and 800 °C/min after a supersolvus solution temperature of 1220 °C for 5 min to dissolve much of the γ', just as illustrated in Fig.1a. For convenience, these samples were subsequently referred by the names of SC (slow cooled), IC (intermediate cooled) and FC (fast cooled). The cooling rates were measured with the aid of thermocouples attached to the specimens and controlled from the solution-treated temperature of 1220 °C to 650 °C. On reaching 650 °C, the specimens were rapidly removed from

the hot zone of the furnace and water-quenched to the room temperature. The interrupted cooling test was composed of several continuous cooling tests, each interrupted test at a different intermediate temperature, just as shown in Fig.1b. Tests were carried out by heating the specimens to a supersolvus solution temperature of 1220 °C, holding for 5 min, and then cooling at 1 °C/min. The cooling process was interrupted at various temperatures and the specimens were subsequently quenched into water rapidly from these temperatures to prevent further changes in the microstructure. For isothermal annealing experiments, specimens were held at 1220 °C for 5 min, cooled down at 1 °C/min to isothermal annealing temperatures held for different times and quenched into water to inhibit further changes in the microstructure, as illustrated in Fig.1c.

For the investigation of morphology and precipitate size evolution of γ' precipitates, samples were observed by a scanning electron microscope (SEM) after electronically etched in 17 mL H_2O +1 mL glacial acetic acid + 2 mL nitric acid solution at 2 V for 20~30 s.

Cylindrical specimens were machined from the bar of 9 mm in height and of 1.5 in height to diameter ratio. The hot compression experiments were conducted under isothermal condition at a constant true strain rate of 0.1 s^{-1} to a true strain of 0.6 s^{-1} at various temperatures. All samples, after homogenous heat treatment, were heated from the room temperature to 1220 °C retained for 5 min, subsequently cooled down to the isothermal temperatures at a cooling rate of 1 °C/min and held for different times before compression tests.

2　Results and Discussion

2.1　Phase transformation analysis and determination of heat treatment

Fig.2 shows the equilibrium phase diagram of the used alloy calculated by Thermo-Calc. According to the diagram, the γ' solvus temperature was approximately about 1175 °C. With decreasing of the temperature, the γ' volume fraction gradually increased under the equilibrium solidification condition. However, due to the fast cooling rate, the equilibrium nucleation and growth of the precipitates were suppressed and the nonequilibrium γ' particles precipitated from the oversaturated γ matrix. In the practice, during supersolvus solution treatment, all primary γ' precipitates remained after forging were dissolved. As the temperature decreased from the solution temperature, upon cooling, some new γ' particles started to precipitate from the matrix. These precipitates formed during the cooling process are defined as the cooling precipitates. In order to understand more comprehensively the development of both the large (secondary) and small (tertiary) γ' during cooling process, an interrupted cooling procedure was carried out. In this procedure, the samples were cooled down at a constant cooling rate and then quenched into water at various interrupted-temperatures. The quenching was required in an at-
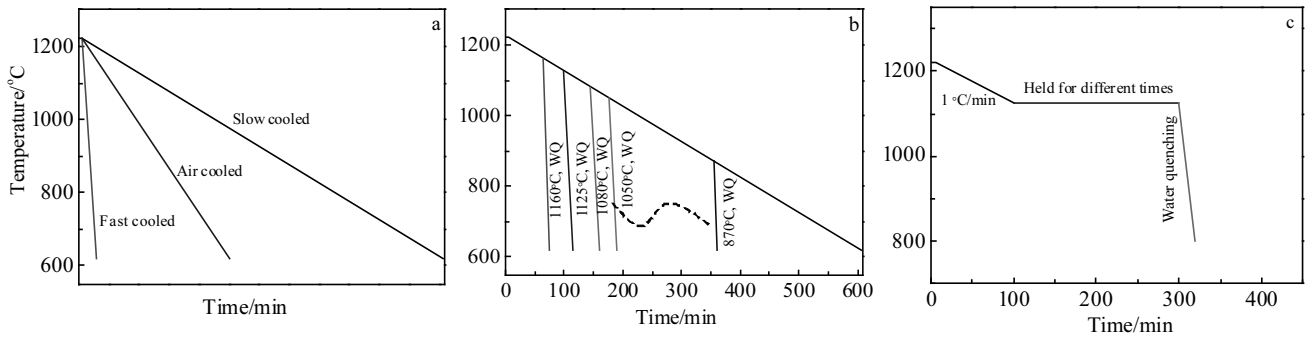
Fig.1 Illustration of continuous cooling (a), interrupted cooling tests (b), and isothermal experiments (c)
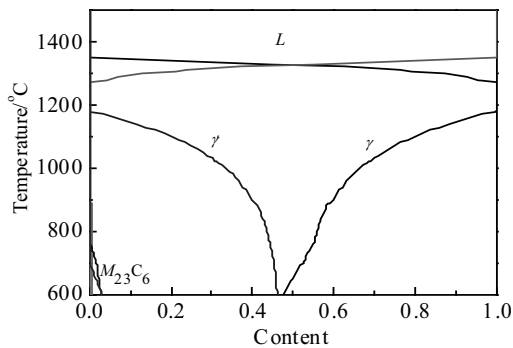

Fig.2 Phase diagram of the alloy predicted by Thermo-Calc

tempt to retain the high-temperature microstructure when the samples were examined at room temperature.

2.2 Precipitate size distribution and morphology evolution

The morphology and size distribution of the cooling precipitates strongly depend on the cooling rates. For the fast cooling rate condition, the microstructure as presented in Fig.3a exhibited a monomodal size distribution of the γ' precipitates of approximately 40 nm in particle diameter. The high density of γ' precipitates observed in this sample was indicative of the corresponding formation at higher undercoolings, where the density of the nucleation sites was expected to

be high. As the cooling rate (IC or SC) decreased, an increase of the precipitate sizes was observed and the size of γ' precipitates still appears to be in monomodal distribution. When the cooling rate was reduced to 1 °C/min, the precipitate shapes changed from spherical to somewhat flowery morphology ones, just as shown in Fig 3c.

Fig. 4 shows the microstructures of the samples that were cooled down linearly at 1 °C/min and water-quenched separately at certain interrupted-temperatures, in an attempt to fully retain the microstructure at the quench initiation temperature. It can be noticed that a monomodal size distribution of the γ' precipitates of about 40 nm was obtained for samples water-quenched at 1160 °C (Fig.4a). The size and morphology of the γ' precipitates were similar to the precipitates produced at the fast cooling rate. A bimodal distribution of the γ' was obtained between the interrupted-temperature range of 1125 and 1100 °C (Fig. 4b and 4c). The size of larger γ' is approximately 250 nm and the size of smaller γ' is about 30 nm. When the temperature decreased to 1050 °C, some γ' particles gathered together and formed flowery particles (Fig.4d). The finer spherical γ' about 10 nm precipitated among the flowery γ' particles. At the temperatures of 960 and 870 °C, only larger flowery γ' particles were observed (Fig. 4e and 4f).

For isothermal annealing experiments, typical microstructures of the samples aged for 2 h at different temperatures are exhibited in Fig.5a~5d. It is interesting that a bimodal distri-
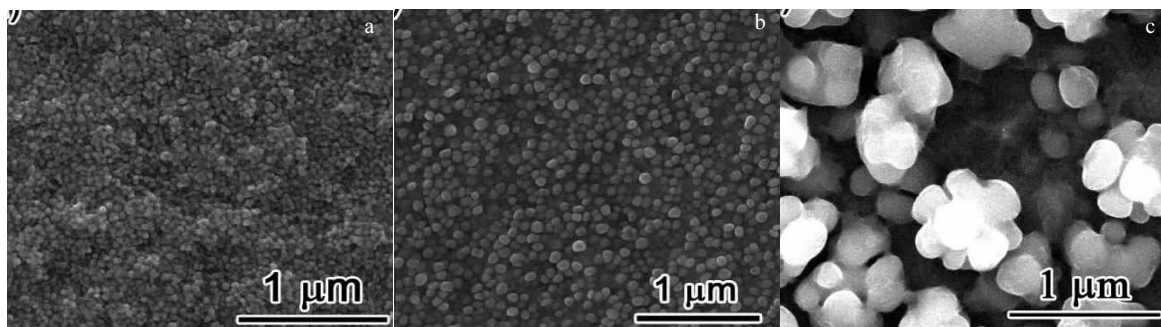

Fig.3 Morphologies of cooling precipitates varying with cooling rates: (a) >800 °C/min, (b) 300 °C/min, and (c) 1 °C/min
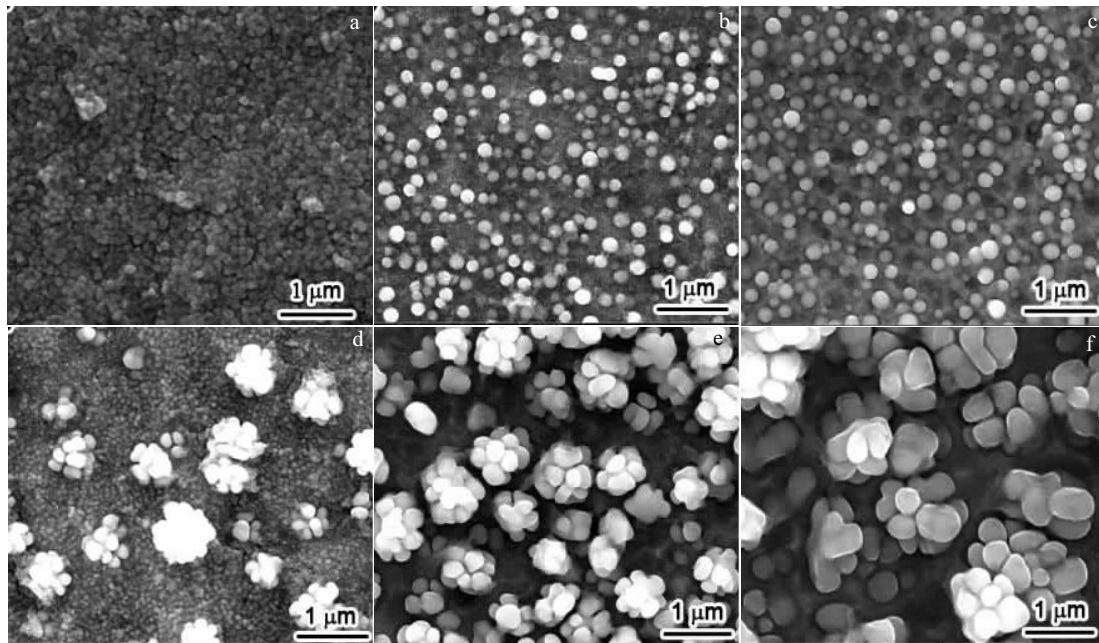
Fig.4 γ' morphology evolution during cooling linearly at 1 °C/min and water-quenched separately at various interrupt-temperatures: (a) 1160 °C, (b) 1125 °C, (c) 1100 °C, (d) 1050 °C, (e) 960 °C, and (f) 870 °C

bution of the γ' precipitates was obtained for the samples annealed beyond 1050 °C and below 1160 °C. The smaller γ' precipitates were approximately 10 nm. A monomodal distribution of the larger γ' was obtained at the intermediate isothermal temperature of 960 °C (Fig.5e). When the temperature was decreased to 870 °C, the tiny γ' particles re-precipitated between the larger γ' precipitates, just as shown Fig. 5f. The microstructural changes along with the aging time at 1125 °C are shown in Fig.6. A bimodal distribution of the γ' precipitates is obvious and the larger γ' particles tend to grow with the increase of aging time.

The precipitation is commonly considered occurring in three distinct steps: nucleation of the new phase through the random formation of supercritical clusters of atoms, growth of these clusters by diffusion transportation of atoms, and finally coarsening, which involves the dissolution of small particles at the expense of large ones. Normally, nucleation, growth and coarsening significantly overlap, in which case the evolutions of particle number density and size depend on all three processes. According to the classical homogeneous nucleation theory, ignoring strain energy, the critical radius to form a stable nucleus is given by[23]

$$ r^* = \frac{-2\sigma}{\Delta G_\upsilon} \qquad (1) $$

where σ is the interfacial energy and ΔG_υ is the chemical volume free energy change driving nucleation. For γ/γ'

two-phase alloy, the volume chemical free energy change ΔG_υ on a nucleus formation can be expressed as[24]

$$ \Delta G_\upsilon = \frac{-R_g T}{V_a} [c_e^{\gamma'} \frac{\ln(c_i)}{\ln(c_e^{\gamma})} + (1 - c_e^{\gamma'}) \frac{\ln(1 - c_i)}{\ln(1 - c_e^{\gamma})}] \qquad (2) $$

where V_a is the molar volume of the precipitating phase, c_i is the instantaneous concentration of solute in the matrix, c_e^{γ} is the concentration of solute in the matrix (γ) in equilibrium with the precipitate (γ') and $c_e^{\gamma'}$ is the equilibrium concentration of solute in the γ' phase. From this equation, it can be seen that the ΔG_υ is mainly relevant to all c_i, c_e^{γ} and $c_e^{\gamma'}$. The ratio between the instantaneous and the equilibrium matrix solute concentration c_i / c_e^{γ} is usually defined as supersaturation[22]. From Eqs.(1) and (2), it is evident that nucleation of γ' depends on two critical factors: one is the chemical free energy provided by the supersaturation in the matrix, and the other is the interfacial energy. That is to say, supersaturation and interfacial energy are the critical parameters in the driving force determination for precipitation. The higher supersaturation results in the higher molar free energy of the γ' precipitates formation and therefore cooling γ' particles can form with a smaller critical size.

For the γ/γ' two-phase alloy, since the shape of the γ-γ' two-phase stability region is asymmetrical [25], just as shown in Fig.7, where the temperature dependence of the γ' equilibrium composition $c_e^{\gamma'}$ within the two-phase field is weak. In contrast, the γ composition c_e^{γ} and c_e^{γ} change significantly

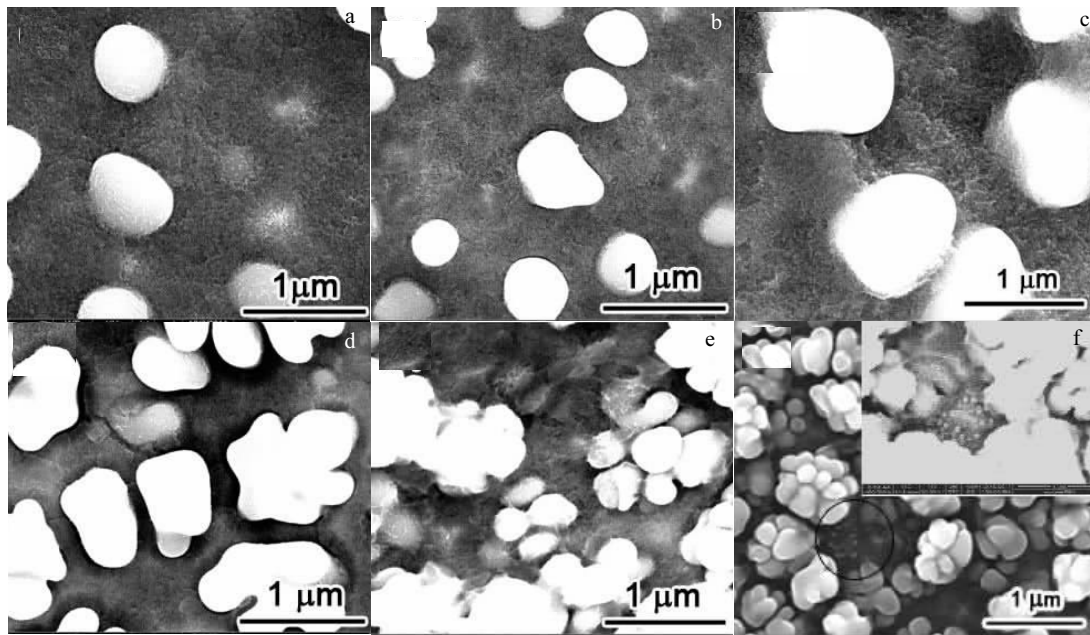Fig.5 γ' morphology evolution of samples subjected to isothermal heat treatments at various temperatures for 2 h: (a) 1160 °C, (b) 1125 °C, (c) 1100 °C, (d) 1050 °C, (e) 960 °C, and (f) 870 °C
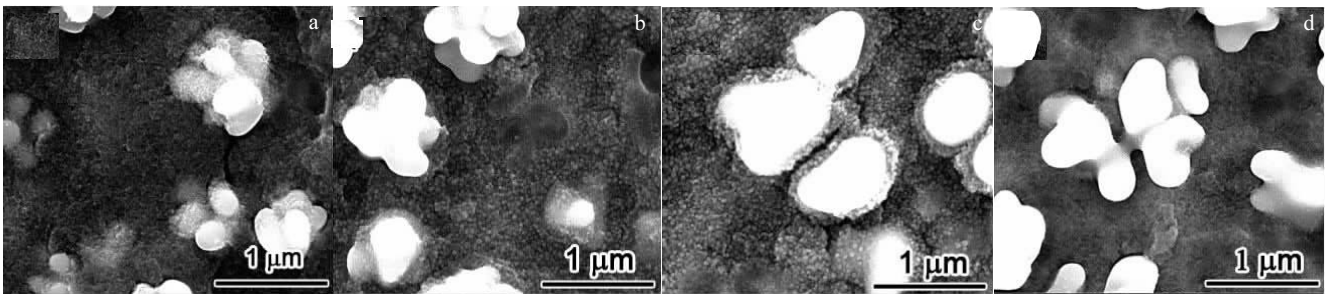

Fig.6 γ' morphology evolution of samples subjected to isothermal heat treatments at 1125 °C for various time: (a) 5 min, (b) 15 min, (c) 30 min, and (d) 120 min
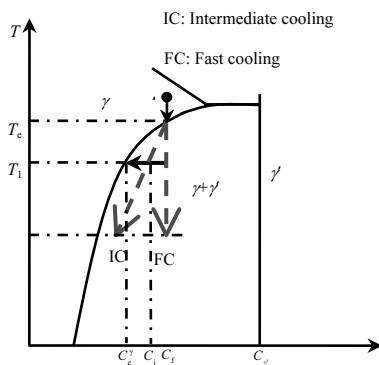

Fig.7   Illustration of Ni-Al phase diagram. Arrows describe thermodynamic paths of alloy during heat treatments consisting of continuous cooling at certain cooling rate from supersolvus-solution temperature to 650 °C

along with temperature. Correspondingly, supersaturation of the γ-matrix can be easily affected by the cooling rate and aging time. For the higher cooling rate, the value of c_i/c_e^γ is higher.

In the current experiments, all heat treatments started with a homogeneous γ phase, which corresponded to an experimental preservation at 1220 °C for 8 h (just as in Fig.7). At a certain cooling rate, the samples were cooled to the temperature (T_1) which is below the equilibrium temperature for the $\gamma\rightarrow\gamma'$ phase transformation, where the γ' precipitates start to nucleate and the first nucleation burst occurs. The γ' precipitates formed in this way will be referred to as the cooling γ' precipitates (or the secondary γ' precipitates). For this alloy, the first-burst nucleation temperature is approximately 1160 °C because some of the γ' particles form during the first burst of nucleation and grow with time under subsequent isothermal annealing at

1160 °C for 2 h, as presented in Fig.5a, which will be explicitly discussed later. For the continuous cooling, regardless of the cooling rates, the monomodal size distribution of the γ' precipitates results from only a single peak of nucleation event, where the nucleation is completely shut down. The sizes of the γ' particles are uniform. It has been reported that the second peak of nucleation occurred at an intermediate cooling rate, which resulted in bimodal particle size distributions[19]. The first burst of nucleation was shut down by a soft impingement accompanied by the secondary γ' precipitates formation; with further cooling, the second peak of nucleation showed up and the tertiary γ' precipitates appeared. However, the present experimental results demonstrate that the tertiary γ' precipitates do not form during the cooling process at an intermediate cooling rate, but rather from the subsequent water quenching. In addition to the size distribution of the γ' precipitates, the size of the γ' particles is mainly related to the supersaturation within the matrix. The evolutions of the precipitates and the matrix composition during the cooling procedure are illustrated in Fig.7, where it is assumed that the quenching or fast cooling is instantaneous. It is shown that the higher cooling rate results in larger supersaturation (c_i/c_e^{γ}) which leads to a higher amount of small-nuclei-size γ' precipitates. If the cooling rate is as small as just about 1 °C/min, the evolution proceeds in a succession of equilibria, where the compositions of the γ matrix and the γ' precipitates follow the limits of the phase diagram at each temperature and consequently the supersaturation is small within the γ matrix. When the temperature decreases to 1160 °C, the secondary γ' precipitates are then formed. With further cooling, certain γ' particles initially grow bigger by the diffusion-controlled growth and some particles dissolve.

For the samples cooled down to the interrupted-temperature at 1 °C/min and then quenched into water, the secondary γ' precipitates produced by the first-burst nucleation will grow due to the slow cooling rate at higher temperature. On the other hand, it is possible to develop the secondary supersaturation in the vicinity of the secondary γ' precipitates if there is enough time for diffusion of alloying elements. It means that the evolution of microstructure during interrupted cooling test should be considered an overlap between nucleation and growth. For the highest interrupt-temperature, the first-burst nucleation of γ' precipitates occurs at 1160 °C and the particles do not have time to grow due to the direct water quenching. The secondary supersaturation around the secondary γ' precipitates is difficult to form, suppressing the tertiary formation during quenching. Therefore, only the monomadal size secondary γ' precipitates are obtained. It should be mentioned that the first-burst nucleation of the γ' precipitates under cooling process occurs at the temperature of 1160 °C since the growth of the secondary γ' precipitates were not observed in the matrix beyond 1160 °C under isothermal aging, whereas for the samples aged at 1160 °C for 2 h, the secondary γ' precipitates

formed by the first burst of nucleation grow in certain areas of the γ-matrix, just as shown in Fig.5a. Therefore, it is certain that the initial precipitation temperature is approximately 1160 °C, lower than the initial precipitation temperature predicted by the Thermo-Calc simulation. In the intermediate interrupt-temperature range (1050 ~ 1125 °C), the first nucleation process comes to a stop and the growth of the secondary γ' precipitates is sufficient. There is a chance for secondary supersaturation to be established again in the vicinity of the secondary γ' precipitates when decreasing the quenching-temperature, leading to the formation of water-quenched tertiaries through the second nucleation burst. Below 960 °C, no tertiaries exist, indicating that the growth rate of the secondary particles is sufficient to deplete the γ'-formed solutes in the matrix and the water-quenching is able to suppress any further tertiary γ' precipitation. It is indicated that the tertiary γ' precipitates form during the post-quenching instead of the continuous cooling through the secondary-burst nucleation. Consequently, at the beginning of quenching beyond 1160 °C, the nucleation plays a dominant role. After the single peak nucleation, the growth of the secondary γ' precipitates dominates the cooling process and the secondary supersaturations are slowly re-established to promote occurrence of the secondary nucleation burst.

It is no doubt that the secondary supersaturation is dependent on the growth of the secondary γ' precipitates. For isothermal annealing between 1050 and 1160 °C, only when the secondary supersaturation sufficiently develops to overcome the energy barrier for a new round of nucleation with the subsequent quenching, does the second-burst nucleation become possible. On the other hand, since the temperature for the second-burst nucleation is too low to allow an intensive solute diffusion, the growth of the tertiary γ' precipitates is restricted. Therefore, the secondary-burst γ' precipitates are much smaller compared to the first-burst γ' particles. As for the aging at 960 °C, the growth rate of the secondary γ' precipitates depletes the solute and suppresses the tertiary formation during quenching, similarly to the interrupted cooling at 960 °C. However, for the tertiary γ' precipitates produced at low temperature of 870 °C, it seems that the low temperature growth rate is sufficiently slow so that supersaturation builds up and leads the tertiary γ' precipitates.

2.3 Effect of isothermal annealing on hot deformation

The typical stress-strain curves obtained at 1125 °C of aging for different times are shown in Fig.8. It is observed that the flow stress rapidly increases to a peak value, and then quickly decreases to a low value. As the strain further increases, the flow stress gradually restores to a steady-state value. Generally, the initial rapid rise in stress is associated with an increase in dislocation density which results in the obvious work hardening[26, 27]. Meanwhile, the dynamic recovery during this stage is too weak to balance the effects of work hardening. As a consequence, the flow stress quickly increases

with the increase of strain. In the softening stage, the accumulated dislocation density exceeds a critical strain, whereas the dynamic recrystallized grains can cause the dislocation annihilation which decreases the flow stress. In the steady stage, the flow stress keeps a steady state due to the dynamic balance between the work hardening and the dynamic softening.

Fig. 9 shows the dependence of the peak stress on aging times at various temperatures. It can be observed that the peak stress decreases with extending aging time. It is reasonable that the decrease of peak stress is caused by the secondary γ' precipitates growth. According to the precipitation hardening[28], when a particle is small, it can be cut by dislocations or weakly coupled dislocation pairs. As the particle increases over a critical size, the Orowan bowing is activated. When a bypass occurs, the strength actually decreases with the increase of the particle size. It has been reported that the critical size for the deformation mechanism changes from the γ'-cutting to Orowan bowing is about 40 nm for a wrought superalloy U720Li[11]. Mao[13] also found a linear decrease of the yield strength with the square root of the mean diameter of the secondary γ' precipitates. The decrease in the peak flow stress in the authors' studies is also believed to rely on the γ'

particles growth. Due to the lower cooling rate, the γ' precipitates formed through the first-burst nucleation grow rapidly to exceed the critical size for deformation mechanism changes before reaching the aging temperature. When aging at the high temperature for different times, the γ' precipitates grow continuously, leading to an increase of the spacing between the secondary γ' particles. Consequently, the peak flow stress starts to decrease by the Orowan bowing mechanism.

3   Conclusions

1) For the continuous cooling test, the size of cooling γ' precipitates increased as the cooling rate decreased and a monomodal size distribution of the γ' precipitates resulted from only a single peak of nucleation event, where the nucleation was completely shut down. With a decrease in cooling rate, the cooling γ' precipitates gradually grew larger and gathered together to form a flowery morphology.

2) In the interrupted cooling experiments, the growth of secondary γ' precipitates was found to occur continuously for the slow cooling rate down to the interrupted temperature below 1125 °C. The tertiary γ' precipitates were formed during water quenching, if the secondary supersaturation was developed in the vicinity of the secondary γ' precipitates. Therefore, the water-quenched tertiary γ' precipitates combined with the secondary γ' particles constituted a bimodal size distribution.

3) The growth effect of secondary γ' particles on the hot deformation was evaluated. The peak flow stress was reduced as the ageing time increased, which might be related to the spacing increase between the secondary γ' particles.
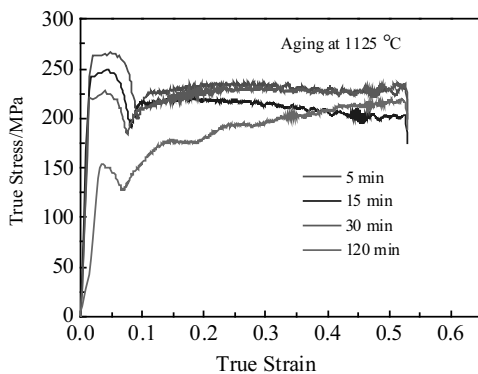

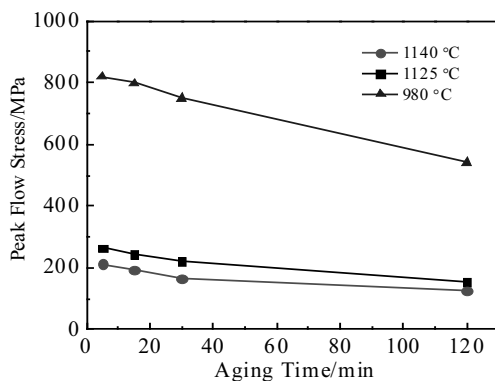Fig.8   True stress-strain curves obtained from compression of used superalloy at 1125 °C aging for various time

Fig.9   Variations of peak flow stress with various aging time for samples compressed at different temperatures

References

1   Nabarro F R N. *Materials Science and Engineering A*[J], 1994, 184(2): 167

2   Pollock T M, Tin S. *Journal of Propulsion and Power*[J], 2006, 22(2): 361

3   Decker R F. *JOM*[J], 2006, 58(9): 32

4   Kovarik L, Unocic R R, Li J *et al. Progress in Materials Science*[J], 2009, 54(6): 839

5   Feller-Kniepmeier, Link T, Poschmann I *et al. Acta Materialia*[J], 1996, 44(6): 2397

6   Bhowal P R, Wright E F, Raymond E L. *Metallurgical Transactions A*[J], 1990, 21(6): 1709

7   Sinharoy S, Virro-Nic P, Milligan W W. *Metallurgical and Materials Transactions A*[J], 2001, 32(8): 2021

8   Shah D M, Duhl D N. *Superalloys 1984*[C]. Warrendale, PA: The Minerals, Metals & Materials Society, 1984

9   Kang S K, Benn R C. *Metallurgical Transactions A*[J], 1985, 16(7): 1285

10 Pope D P, Ezz S S. *International Metals Reviews*[J], 1984, 29(1): 136

11 Jackson M P, Reed R C. *Materials Science and Engineering A*[J], 1999, 259(1): 85

12 Torster F, Baumeister G, Albrecht J *et al. Materials Science and Engineering A*[J], 1997, 234-236(30): 189

13 Mao J, Chang K, Yang W *et al. Metallurgical and Materials Transactions A*[J], 2001, 32(10): 2441

14 Kozar R W, Suzuki A, Milligan W W *et al. Metallurgical and Materials Transactions A*[J], 2009, 40(7): 1588

15 Singh A R P, Nag S, Hwang J Y *et al. Materials Characterization*[J], 2011, 62(9): 878

16 Furrer D U, Fecht H. *Scripta Materialia*[J], 1999, 40(11): 1215

17 Radis R, Schaffer M, Albu M *et al. Acta Materialia*[J], 2009, 57(19): 5739

18 Sarosi P M, Wang B, Simmons J P *et al. Scripta Materialia*[J], 2007, 57(8): 767

19 Wen Y H , Simmons J P, Shen C *et al. Acta Materialia*[J], 2003, 51(4): 1123

20 Safari J, Nategh S, McLean M. *Materials Science and Technol-ogy*[J], 2006, 22(8): 888

21 Robson J D. *Materials Science and Technology*[J], 2004, 20(4): 441

22 Robson J D. *Acta Materialia*[J], 2004, 52(15): 4669

23 Schwarz R B, Labusch R. *Journal of Applied Physics*[J], 1978, 49(10): 5174

24 Aaronson H I, Laird C, Kinsman K R. *Phase Transformations*[M]. Metals Park, OH: American Society of Metals, 1970

25 Wang J, Osawa M, Yokohawa T *et al. Superalloys 2004*[C]. Warrendale, PA: The Minerals, Metals & Materials Society, 2004

26 Chen X, Lin Y C, Wen D *et al. Materials & Design*[J], 2014, 57(15): 568

27 Yuan H, Liu W C. *Materials Science and Engineering A*[J], 2005, 408(1-2): 281

28 Lin Yijian, Cahn R W. *Physica Status Solidi*[J], 1992, 131(2): 481

镍基变形高温合金中 γ′相的多尺度分布行为及其对热变形性能的影响

韩国明 [1]，李 飞 [1]，孙宝德 [1,2]

(1. 上海交通大学 上海市先进高温材料及其精密成形重点实验室，上海 200240)

(2. 上海交通大学 金属基复合材料国家重点实验室，上海 200240)

摘　要：主要研究了镍基变形高温合金在不同热处理过程中 γ′相的析出、形貌、尺寸及分布行为。通过扫描电镜观察分析高温固溶热处理后连续冷却、中断固溶冷却以及等温时效淬火后的组织构成。结果表明，固溶处理后连续冷却过程中，当冷却速率较高时，二次 γ′尺寸大小均匀，呈现单峰分布，随着冷却速率降低，二次 γ′尺寸增加，逐渐聚集长大并呈现花状形貌；在等温时效过程中二次 γ′周围过冷度重新建立，随后淬火过程中会产生三次 γ′，三次 γ′与二次 γ′构成双峰分布。在此基础上，探讨了 γ′相析出及演化对合金热变形行为的影响。

关键词：变形高温合金；γ′相；热处理；热变形

作者简介：韩国明，男，1982 年生，博士后，上海交通大学，上海 200240，电话：021-34202951，E-mail: gmhan@sjtu.edu.cn